http://dx.doi.org/10.2139/ssrn.4867777 SSRN Preprint

Ozone variations over Antarctic stations during sudden stratospheric warmings

Ruixian Yu[1], Asen Grytsai[2,3], Alina Burmay[2], Gennadi Milinevsky[1,3,*], Oleksandr Evtushevsky[2], Andrew Klekociuk[4,5], Yu Shi[6,**], Oleksandr Poluden[3], Xiaolong Wang[6], Oksana Ivaniha[7]

[1]College of Physics, International Center of Future Science, Jilin University, 2699 Qianjin Str., Changchun 130012, China
[2]Taras Shevchenko National University of Kyiv, 60 Volodymyrska Str., Kyiv 01601, Ukraine
[3]State Institution National Antarctic Scientific Center, 16 Taras Shevchenko Blvd., Kyiv 01601, Ukraine
[4]Australian Antarctic Division, 203 Channel Highway, Kingston, Tasmania 7050, Australia
[5]School of Physics, Chemistry and Earth Sciences, University of Adelaide, 10 Pulteney Str., Adelaide 5005, Australia
[6]College of Electronic Science and Engineering, International Center of Future Science, Jilin University, 2699 Qianjin Str., Changchun 130012, China
[7]Earth Physics and Astrophysics Department, Universidad Complutense de Madrid, 2 Séneca Ave., Madrid 28040, Spain

Corresponding authors at: College of Physics, International Center of Future Science, Jilin University, 2699 Qianjin Str., Changchun 130012, China.
E-mail address: *milinevskyi@jlu.edu.cn, genmilinevsky@gmail.com (G. Milinevsky).
College of Electronic Science and Engineering, International Center of Future Science, Jilin University, 2699 Qianjin Str., Changchun 130012, China.
E-mail address: **shiyuy@jlu.edu.cn (Y. Shi).

Abstract. Understanding the connection between sudden stratospheric warmings (SSW) and variations in the zonally asymmetric response of the total ozone column (TOC) has application in better anticipating regional variations in surface ultraviolet radiation at extratropical latitudes. Here we examine the evolution of three SSW events in the Southern Hemisphere (SH) in September 1988, 2002 and 2019 which reveals new features of the zonally asymmetric response of TOC to SSW events. Our analysis is based on MSR-2 TOC data presented as time series for ten stations in the Antarctic and the sub-Antarctic region, and as a gridded field for the SH. We use superimposed epoch analysis for ±60 days relative to the central date of SSW, and the regional division of the time series between the Western and Eastern Hemispheres according to the climatological TOC asymmetry. The average zonally asymmetric response of TOC to the SSWs is characterized by generally stronger (weaker) positive anomalies in the Eastern (Western) Hemisphere, with the anomaly maximum occurring on day 0 (day +5). Synchronized anomalies are observed in the two hemispheres between day +5 and day +15 with a joint minimum near day +10 that is associated with a decrease in the amplitude of zonal wave 1 at 60°S and 50 hPa deduced from MERRA-2 reanalysis. During each SSW, stratospheric ozone depletion (ozone hole region) and accumulation (ozone collar region) impose differences in the latitude–longitude-depended TOC responses at Western (weaker) and Eastern (stronger) Hemisphere stations. The asymmetric TOC pattern is formed due to zonal wave 1 which displaces the ozone hole from the South Pole. The pattern is further enhanced by zonally asymmetric accumulation of ozone in the collar region. The time scale of synchronized wave and ozone variations during the SSW main stage in our composites is 10–15 days and the variations are quasi-periodic within a 120-day interval.

Keywords: total ozone column, Antarctic research stations, MSR-2 overpass data, sudden stratospheric warming, planetary waves

1 Introduction

A sudden stratospheric warming (SSW) can influence a significant bulk of the extratropical atmosphere, affecting not only the stratosphere (Matsuno, 1971; Schoeberl, 1978; Butler et al., 2015; Baldwin et al., 2021), but also the troposphere, including the surface layer (Domeisen and Butler, 2020; Shi et al., 2024a), and the mesosphere (Chandran and Collins, 2014; Eswaraiah et al., 2023). The most noticeable effect of a SSW is observed in the polar stratosphere, where the temperature can rise by tens of degrees, which is accompanied by a decrease in the speed of the westerly circulation or even its change to become easterly. For characterizing SSWs, the terms of minor, major, and final warmings have been proposed (Butler et al., 2015). A major SSW is separated from minor events by requiring a reversal of the zonal wind to easterly at 10 hPa pressure level (~32 km height) at 60° latitude (Butler et al., 2015; Baldwin et al., 2021). During a SSW, the stratospheric polar vortex can shift from the pole or split into two parts (Hirota et al., 1990; Newman and Nash, 2005; Charlton and Polvani, 2007; Chandran and Collins, 2014). In this regard, the thermal impact on the midlatitude stratosphere can be significant, as the cold and ozone-poor polar air masses in the vortex remnants shift from their usual position to lower latitudes.

SSWs are a common phenomenon in the Arctic where such events occur approximately every other winter (Charlton and Polvani, 2007; Butler et al., 2015). Fairly frequent SSW events in the Northern Hemisphere (NH) allow their statistical description depending on event strength (minor – major), type (vortex displacement – vortex split, or wave 1 – wave 2 dominant impact), lifecycle, phase, or frequency (Hitchcock et al., 2013; Butler et al., 2015; Baldwin et al., 2021; Shen et al., 2022). In the Southern Hemisphere (SH) over Antarctica, SSWs are much rarer because the stratospheric polar vortex is more stable, which is due to lower activity of Rossby (planetary) waves (Kanzawa and Kawaguchi, 1989; Butler et al., 2015; Wang et al., 2020; Jucker et al., 2021).

Historically, only three notable SSW events have occurred in the SH and each of them has attracted much attention from researchers. These were minor warmings in September 1988 (Kanzawa and Kawaguchi, 1989; Schoeberl et al., 1989; Hirota et al., 1990; Grytsai et al., 2008; Roy et al., 2022) and 2019 (Milinevsky et al., 2020; Safieddine et al., 2020; Shen et al., 2020; Lim et al., 2021; Roy et al., 2022; Veenus and Das, 2024) and major warming in September 2002 (Varotsos, 2002; Allen et al., 2003; Baldwin et al., 2003; Newman and Nash, 2005; Charlton et al., 2005; Grytsai et al., 2008; Roy et al., 2022; Mitra and Guharay, 2024). These are the years of the historically lowest ozone loss in the Antarctic spring (Roy et al., 2022).

The cause of the major SSW 2002 event was very strong activity of stationary planetary wave with zonal wave number 2 (wave 2), which led to the splitting of the polar vortex into two circulation cells. During this event, an increase in polar temperatures by 30 K over a week penetrated deeply to the lower stratosphere and upper troposphere (Varotsos, 2002; Newman and Nash, 2005; Kozubek et al., 2020).

The SSWs of 1988 and 2019, which are classified as minor type events, were accompanied by an exceptionally strong planetary wave with zonal wave number 1 (wave 1), a large polar vortex displacement, and a significant increase in polar stratospheric temperatures by about 60 K in 10 days and by 50 K in a week, respectively, which affected mainly the middle and upper levels (Hirota et al., 1990; Lim et al., 2021; Roy et al., 2022). For comparison, climatological temperature anomalies in the NH near the central date of SSWs typically reach +15 K in the middle stratosphere and can eventually reach 50–60 K (Schoeberl, 1978; Baldwin et al., 2021).

The three SH SSWs produced changes in the distribution of ozone that were associated with disturbed thermal and dynamical conditions in the Antarctic stratosphere produced by enhanced planetary wave activity. An important role in anomalies of the total ozone column (TOC) is played by the Brewer–Dobson Circulation (BDC), which provides poleward transport of ozone from the tropics and its subsequent downwelling over the extratropics (Weber et al., 2011; Butchart, 2014; Veenus and Das, 2024). Approximately 90% of the TOC is confined to the altitude range 15-35 km, and the distribution of ozone at these heights is dictated by transport processes because its photochemical lifetime in the absence of chemical depletion is on the order of weeks to months. Because quasi-stationary wave 1 is dominant in the SH stratosphere, both the stratospheric polar vortex (Waugh and Randel, 1999; Charlton et al., 2005) and the BDC-related ozone transport towards Antarctica (Sato et al., 2009; Agosta and Canziani, 2010; Gabriel et al., 2011) are zonally asymmetric. The large-scale waves produce eddies in the circulation with wind components that influence the poleward and vertical movement of ozone. A zonal TOC minimum is formed in the Western Hemisphere (WH) in the Atlantic longitude sector and around the Greenwich meridian due to the off-pole displacement of the ozone hole (Wirth, 1993; Malanca et al., 2005; Grytsai et al., 2017; Shen et al., 2022). A zonal TOC maximum exists in the Eastern Hemisphere (EH) in the so-called ozone "collar" region (Mariotti et al., 2000) covering mainly midlatitudes in the Australian longitude sector (Wirth, 1993; Grytsai et al., 2007; Ialongo et al., 2012).

Since the early 1980s, ozone depletion associated within the so-called ozone hole has caused a significant perturbation in TOC over Antarctica in the austral spring (Stolarski, 1988; Newman et al., 2004). After the annual disappearance of the ozone hole and the final stratospheric warming, which generally occurs in late spring or early summer, TOC increases over Antarctica due to the mixing of the ozone-poor polar air with the ozone-enriched air of the midlatitude ozone collar region (Allen et al., 2003; Safieddine et al., 2020; Baldwin et al., 2021; Roy et al., 2022). Then, usually from December to the following August, TOC levels return to the typical climatological seasonal cycle (Fioletov and Shepherd, 2003). Strong changes in TOC during minor or major SSWs disrupt the typical TOC decline during the ozone hole season, as BDC enhancement and vortex disturbance and warming lead to an increase in stratospheric ozone and a reorganisation of its spatial pattern over Antarctica (Varotsos, 2002; Baldwin et al., 2003; Newman and Nash, 2005; Grytsai et al., 2008; Veenus and Das, 2024). These dynamical influences on Antarctic ozone are of great importance for local observations. The measured TOC variations depend significantly on the location of the research station under the perturbed TOC field (Farman, 1987; Pazmiño et al., 2005; Agosta and Canziani, 2010; Hassler et al., 2011). However, to what extent, with such a dependence, TOC variations at different Antarctic stations differ or have common features during SSW, is still little studied (Pazmiño et al., 2005; Klekociuk et al., 2021). In this work, we compare TOC time series at ten Antarctic and sub-Antarctic stations using their lagged composites relative to the central dates of SSWs 1988, 2002 and 2019. The aim is (i) to analyze the impact of SSW evolution on TOC variation compared to climatological seasonal changes, and (ii) to clarify whether there are common SSW manifestations in spatially dependent ozone observations under the zonally asymmetric TOC field.

The MSR-2 and MERRA-2 reanalysis data are used as described in Section 2. In Section 3, we analyze the local TOC climatology at ten stations taking into account zonal TOC asymmetry and present the result of the analysis of SSW effects using the superimposed epoch method. A discussion is given in Section 4, followed by conclusions in Section 5.

2 Data and method

We have processed total ozone column data from the Multi Sensor Reanalysis version 2 (MSR-2) for the period 1979–2022 that are presented as timeseries for eight Antarctic and two sub-Antarctic research stations (Van der A et al., 2015; https://temis.nl/protocols/o3field/overpass_msr2.php). The station locations are given in Table 1 and Fig. 1 and Fig. 2.

Two sub-Antarctic stations are Ushuaia (Argentina) on the southern edge of South America and Macquarie (Australia) on an island halfway between Tasmania and Antarctica. According to the geographic location (Fig. 1) and TOC climatology described below in Section 3.1 (Fig. 2), and the stations listed in the left and right columns of Table 1 are hereafter referred to as Western Hemisphere (WH) and Eastern Hemisphere (EH) stations, respectively.

Table 1. Coordinates of ten research stations in Antarctica and the sub-Antarctic included in the analysis of the TOC response to sudden stratospheric warming. The MSR-2 overpass data are used.

South Pole and Western Hemisphere			Eastern Hemisphere		
Name	Lat	Long	Name	Lat	Long
Amundsen-Scott	90.0°S	139.3°E	Syowa	69.01°S	39.59°E
Neumayer	70.62°S	8.37°W	Zhongshan	69.4°S	76.4°E
Rothera	67.6°S	68.1°W	Davis	68.6°S	78.0°E
Faraday/Vernadsky	65.24°S	64.25°W	Dumont d'Urville	66.7°S	140.0°E
Ushuaia	54.8°S	68.3°W	Macquarie	54.5°S	158.9°E

The onset dates of the sudden stratospheric warming events were taken from (Shen et al., 2020), where the maximum temperature during the early stage of the SSW events was determined as 28 September 1988, 29 September 2002, and 19 September 2019. Supplementary Fig. S1 illustrates zonal mean air temperature at 10 hPa in the latitude–time sections using the NCEP–NCAR reanalysis (Kalnay et al., 1996; https://psl.noaa.gov/map/time_plot/). The SSW central dates are indicated by solid horizontal lines. These SSW events occur typically as a series of warmings (Newman and Nash, 2005; Roy et al., 2022), and central date for the second minor warming of 19 September 2019 was selected (Fig. S1c) as the date when the highest temperature was reached (Shen et al., 2020).

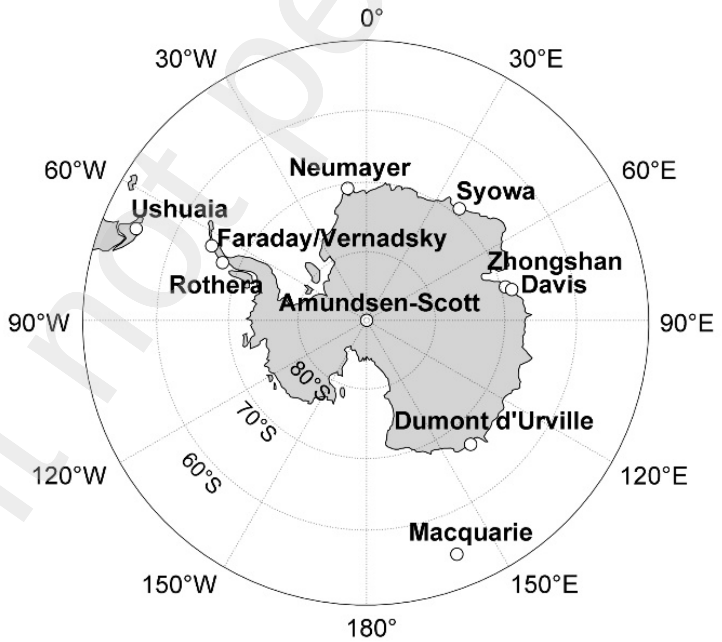

Figure 1. Map of the location of research stations listed in Table 1.

A superimposed epoch method, also known as composite analysis (Xie et al., 2017), was used in which the listed SSW dates were selected as day 0 in the time-lagged composite analysis. The TOC values at each station were averaged over three SSW events for each day within ±60 days relative to day 0, i.e., two months before (negative time lag) and two months after (positive time lag) the central SSW date. The presence of a seasonal variation of TOC is a systematic factor that, in the first approximation, can be eliminated by a simple procedure. First, we determined the daily TOC climatology using MSR-2 data for 1979–2022. Then deviations of TOC from climatology (TOC anomalies) were considered using the composite analysis method. For day 0 in the lagged composites for climatology, the mean of the central dates of the three events (25 September) was chosen. This date is within −6 days to +4 days away from the individual SSW dates, which is a relatively small offset (3–5%) compared to the ±60-day time scale. Considering the slow seasonal change of TOC in climatology (red curves in Figs. S2 and S3), this choice does not significantly affect the magnitude of daily variations in TOC anomalies.

The MERRA-2 reanalysis was used to examine variations in the amplitudes of zonal wave 1 and wave 2 in geopotential height (Gelaro et al., 2017; https://acd-ext.gsfc.nasa.gov/Data_services/met/ann_data.html). In order to compare MSR-2 assimilated ozone data with ground-based observations, TOC time series measured at Faraday/Vernadsky (Dobson measurements) and Dumont d'Urville (WOUDC Système d'Analyse par Observation Zénithale data, https://woudc.org/data/explore.php, Hendrick et al., 2011) were used.

In a study where there are very few events, which is the case for the Southern Hemisphere, then it can be expected that the role of random factors during averaging will at least decrease, and the general properties deduced from the average will turn out to be much more reliable than basing conclusions on the properties of any randomly selected event. In the study of three events considered here, averaging of the TOC anomalies can help show whether there are common properties in time relative to the central date of stratospheric warming.

3 Results

3.1 September patterns of TOC in climatology and SSW years

Since all three anomalous warmings in the Antarctic stratosphere have occurred in September, we illustrate the TOC patterns specific to this month using the 1979–2022 climatology and monthly means of 1988, 2002 and 2019 (Fig. 2). The maps in Fig. 2 show the presence of two TOC extremes, which are located asymmetrically with respect to the South Pole, as noted in Section 1. In the climatology, the zonal TOC minimum is shifted relative to the South Pole and the 60°S latitude circle into the WH towards South America and the Atlantic sector (dashed arrow and black dashed and solid contours 220 and 280 Dobson Units (DU) in Fig 2a). It has an almost circular shape, and the absence of a noticeable elongation indicates the insignificant contribution of wave 2 and the dominance of wave 1 in the climatology of September (Fig 2a). The zonal TOC maximum occupies mainly the sub-Antarctic region in the EH in the longitudinal sector of Australia (white solid contour 380 DU in Fig. 2a). Increased TOC levels above 330 DU are observed throughout the 30–60°S zone in the form of ozone collar (Mariotti et al., 2000). The existence of two TOC extremes confirms the climatological dominance of zonal wave 1 in the September TOC pattern.

It is seen from the black solid 280 DU contour that the zonal TOC minimum for the warmer stratospheres of September 1988, 2002 and 2019 takes a smaller area (Fig. 2b–2d) than the climatological average (Fig. 2a). The ozone hole is defined by the TOC less than 220 DU, which were not observed prior to 1979, while after 1979 numerous observations showed values below 220 DU (Newman et al., 2004). The monthly mean ozone hole area in September of the SSW years undergoes an especially notable decrease when compare to the climatology (black dashed contour 220 DU in Fig. 2b–2d and Fig. 2a, respectively). The TOC minimum area in the SSW years is more shifted off the pole, elongated and rotated westward (black solid contour 280 DU and arrows in Fig. 2b–2d). Elongation and rotation are due to the activity of stationary wave 2 in SSW events and its interaction with wave 1, which leads, in particular, to a phase shift of the combined wave to the west (Grytsai et al., 2007; 2008). Since the ozone poor air is inside the stratospheric polar vortex, the interaction of amplified waves with zonal mean flow at the vortex edge is mostly reflected in the ozone hole shape, size and location, as seen from Fig. 2b–2d (black dashed contour 220 DU).

Considering the zonal TOC maximum located outside the polar vortex, the anomalous Septembers are characterized by a significant increase in the peak levels to about 450 DU (white dashed contour in Fig 2b and 2d). Additionally, a spatial extension along the 30–60°S zone increases almost to the EH scale (white solid contour 380 DU in Fig 2b–2d) compared to climatology (Fig. 2a). As a result of a spatial expansion, the zonal maximum partially overlaps the eastern edge of the Antarctic continent. This affects the observed TOC levels at the EH stations (Fig. 2b–2d) located at 67–70°S (Fig. 1 and Table 1).

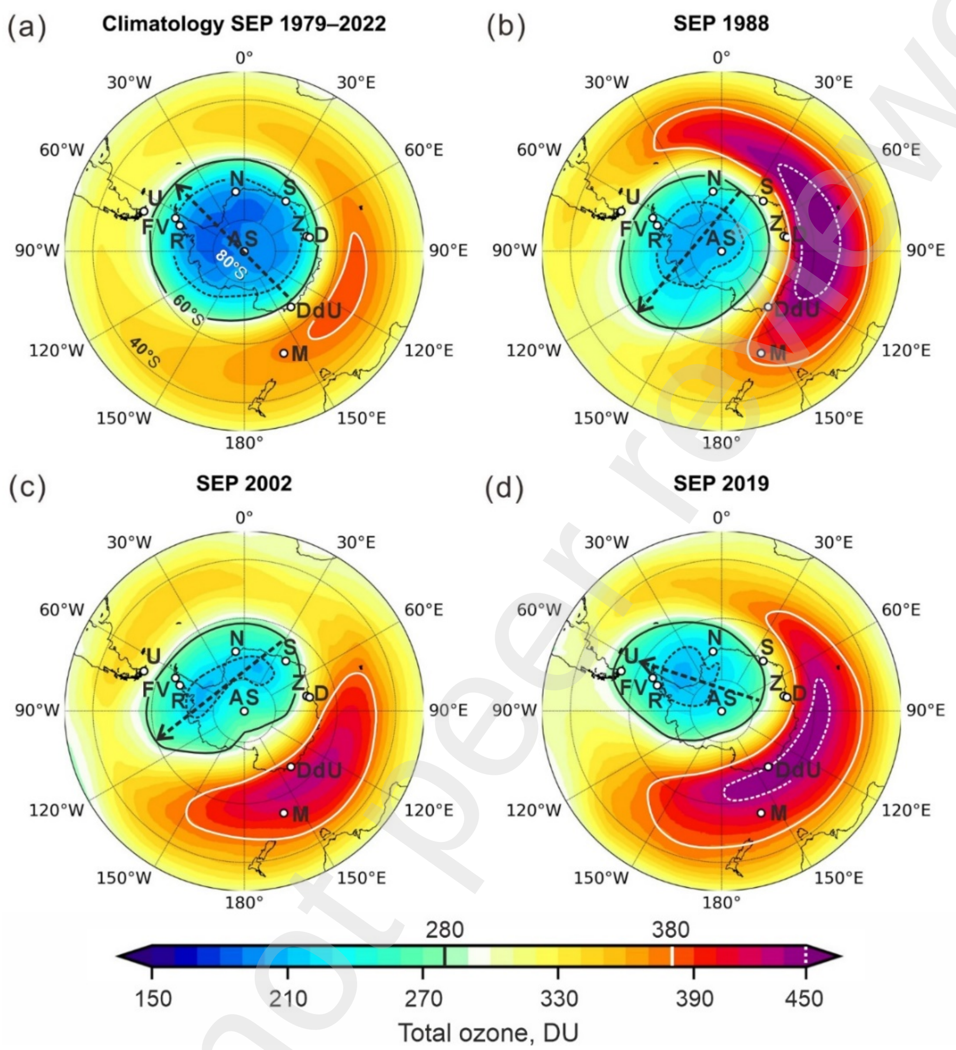

Figure 2. Zonal TOC asymmetry in September by (a) climatology 1979–2022 and monthly means in SSW years (b) 1988, (c) 2002 and (d) 2019. Black dashed and solid contours are at the zonal TOC minimum levels of 220 DU (ozone hole edge) and 280 DU, respectively. Dashed arrow indicates axis of the elongated TOC minimum area. White solid (dashed) contour outlines zonal maximum region at 380 DU (450 DU). The MSR-2 data are used. Abbreviations of station names: AS – Amundsen–Scott, U – Ushuaia, FV – Faraday/Vernadsky, R – Rothera, N – Neumayer, S – Syowa, Z – Zhongshan, D – Davis, DdU – Dumont d'Urville, and M – Macquarie.

Climatologically, seven Antarctic stations, namely Amundsen–Scott, Faraday/Vernadsky, Rothera, Neumayer, Syowa, Zhongshan, and Davis (AS, FV, R, N, S, Z, and D, respectively, in Fig. 2) are permanently surrounded by low TOC levels from <220 DU to about 250 DU (Fig. 2a). The stations of Dumont d'Urville (DdU) and Ushuaia (U) fall into the area of intermediate TOC levels near 300 DU, while Macquarie (M) is persistently affected by the zonal TOC maximum at about 370 DU (Fig. 2a). During the anomalous warming of the Antarctic stratosphere, when the area of the zonally asymmetric ozone minimum is reduced significantly and shifted from the pole, five stations (AS, N, R, FV and U) are more likely to be in the region of lowest TOC. The remaining five stations Syowa (S), Zhongshan (Z), Davis (D), Dumont-d'Urville (DdU) and Macquarie (M) may be more frequently affected by high TOC. Consistent with the zonal TOC asymmetry in Fig. 2, the stations that fall into the regions of the zonal minimum and zonal maximum are hereinafter referred to as the WH and EH stations, as listed in Table 1. As shown below, the daily TOC time series and TOC fields show much greater variability, and the monthly mean data for September in Fig. 2 will serve here as a reference distribution of TOC in the analysis of its variability during the stratospheric warmings.

The daily climatology of TOC is presented separately for the station groupings of WH (Fig. 3) and EH (Fig. 4) using the MSR-2 timeseries. The five stations of Fig. 3 are strongly influenced by the regions of TOC minimum and TOC maximum, respectively. The deep TOC minimum over the Antarctic stations in Fig. 3a–3d appears in September–October (days 250–300) due to the formation of the spring ozone hole. Although to a much lesser extent, the effect of the displaced ozone hole is also visible at the midlatitude station Ushuaia with the TOC decrease of about 20 DU (Fig. 3e). This effect is associated with the proximity of the ozone hole edge to the station and frequent intrusions of low ozone polar air in conditions of increased wave activity in spring (Muostaoui et al., 2003; Pazmiño et al., 2005; Agosta and Canziani, 1010; see also Fig. 2).

There is a clear latitudinal sequence (from the pole to lower latitudes) in an increase of both maximum and minimum TOC levels. For example, the spring minima are 150, 170, 200, 230 and 300 DU at stations AS, N, R, FV, and U, respectively (Fig. 3a–3e). The latitude-dependent effect of the ozone hole is reflected in the range of TOC decline between the winter maximum and spring minimum, decreasing equatorward (Fig. 3a–3d): 110 DU (AS and N), 90 DU (R), and 70 DU (FV).

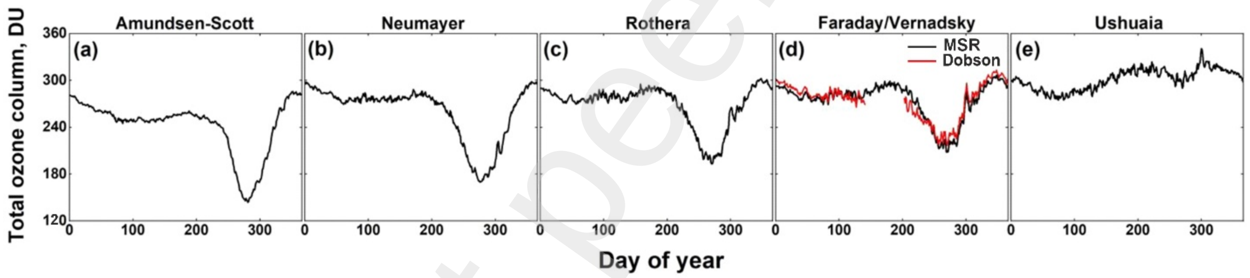

Figure 3. Daily TOC climatology 1979–2022 for (a) Amundsen–Scott South Pole station, and the Western Hemisphere Antarctic stations in sequence from higher to lower SH latitudes (Table 1): (b) Neumayer, (c) Rothera, (d) Faraday/Vernadsky, and (e) the sub-Antarctic station Ushuaia. MSR-2 data are used (black line); the red line in (d) shows climatology based on the Dobson observations at Faraday/Vernadsky.

A similar latitudinal sequence is observed from the time series for the EH Antarctic stations (Fig. 4a–4d). Because of the closeness of the ozone collar maximum, the TOC decline range is lower, than that in WH, and is of 90 DU (S), 60 DU (Z and D), and 30 DU (DdU). The impact of the ozone hole at midlatitude station Macquarie is completely absent. The seasonal TOC cycle here exhibits a clear spring maximum, and peak values reach about 390 DU (Fig. 4e) against 320 DU at Ushuaia (Fig. 3e). The spring maximum at Macquarie is typical for the annual tendency in the midlatitude TOC of both hemispheres (Fioletov and Shepherd, 2003).

Thus, Figs. 2–4 show that the quasi-stationary zonal minimum and maximum of TOC determine the mean levels and range of the annual TOC changes when observed locally in September in high and middle southern latitudes. Contributions from the ozone hole and ozone collar regions are manifested in generally lower TOC levels in WH than in EH, respectively. As we will discuss in the next section, anomalous wave activity during SSWs perturbs these patterns and affects the longitude–latitude dependence of local TOC levels.

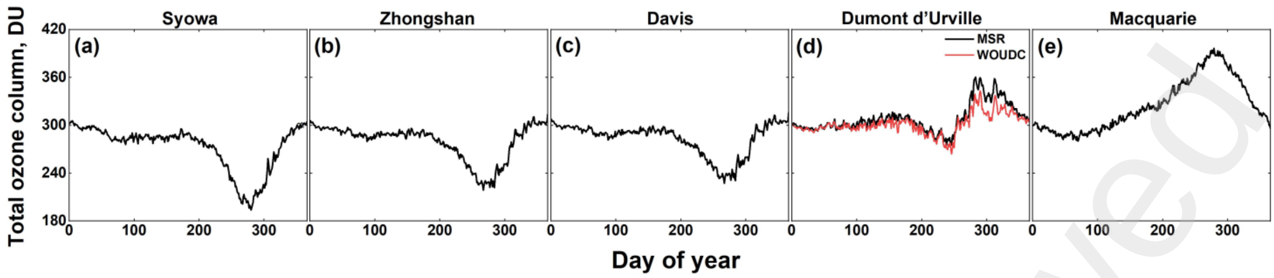

Figure 4. Daily TOC climatology 1979–2022 for Eastern Hemisphere Antarctic stations in sequence from higher to lower SH latitudes (Table 1): (a) Syowa, (b) Zhongshan, (c) Davis, (d) Dumont d'Urville and (e) sub-Antarctic station Macquarie. MSR-2 data are used (black line); the red line in (d) shows the climatology based on WOUDC datasets for Dumont d'Urville.

3.2 Local TOC responses averaged over three SSW events

In this section, the impacts of three SSWs of 1988, 2002 and 2019 on the TOC anomalies over the ten stations are examined using MSR-2 overpass data. The MSR-2 data are provided at 6-hourly intervals for 00 UT, 06 UT, 12 UT, 18 UT. We used data for 12 UT to represent the daily measurements over each station. Variations of the TOC anomalies relative to the 1979–2020 climatology were analyzed using the method of superimposed epochs with a ±60-day time lag and three-event averaging (Fig. 5 and Fig. 6). With the same time lag, TOC variations at all ten stations in individual events and in climatology are shown in Figs. S2 and S3.

At WH stations, relatively small-amplitude anomaly variations of ±40 DU were present in the pre-SSW period (Fig. 5). The largest positive anomaly of about 140 DU appeared around day 0 at Amundsen–Scott (Fig. 5a) and it was mainly contributed by SSW 2002, when TOC maximized near 400 DU (green dotted curve in Fig. S2). Large anomalies of 80–120 DU were raised at Rothera, Faraday/Vernadsky and Ushuaia after each SSW within about a 20-day time lag (Fig. 5c–5e), with the most significant contribution coming from SSW 2002 (green dotted curves in Fig. S2c–S2e). Almost indistinguishable on the background of the daily variations, but centered on day 0, is a small anomaly at Neumayer (Fig. 5b) of 40 DU in maximum excursion. As distinct from other WH stations, Neumayer was under the low-variable TOC level at about 250 DU in all three events near day 0 (Fig. S2b), as well as and in the monthly means in September (N in Fig. 2b–2d).

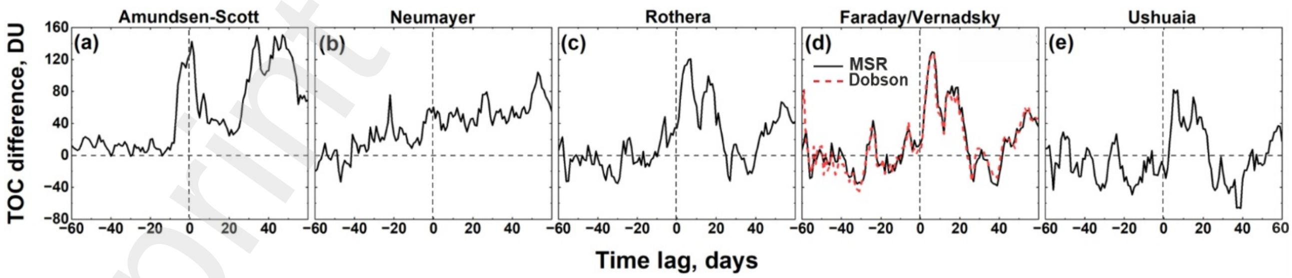

Figure 5. The TOC anomalies relative to the climatology 1979–2022, averaged over three SSW years for stations (a) Amundsen–Scott, (b) Neumayer, (c) Rothera, (d) Faraday/Vernadsky and (e) Ushuaia. The method of superimposed epochs with ±60-day time lag relative to the SSW central date was used. MSR-2 data are used (black line); the red line in (d) shows anomalies based on the Dobson observations at Faraday/Vernadsky.

It should be noted that there is generally less (more) frequent occurrence of positive (negative) anomalies with decreasing station latitude (between Fig. 5a and 5e). The region of the lowest TOC in the anomalous September is shifted from the pole into the WH further (Fig. 2b–2d) than in the climatology (Fig. 2a), which may account for the observed latitudinal dependence in the negative anomaly frequency. At the same time, the region of the highest TOC is in the opposite EH, and increasing the distance of the zonal minimum region from the pole in anomalous September reduces the probability of negative anomalies at the EH stations (Fig. 6). Nevertheless, to varying degrees, the SSW effect with positive TOC anomalies near or after day 0 is present at all stations. This effect at the EH Antarctic stations also stands out in the anomaly variations (Fig. 6a–6d), but not as sharply as at the WH stations and the South Pole (Fig. 5).

The highest positive peaks of about 160 DU are near the central date at Zhongshan, Davis and Dumont d'Urville (Fig. 6b–6d) and are much higher than at Amundsen-Scott and other WH stations (Fig. 5). This indicates that significant ozone accumulation in the extended ozone collar region in the SSW years is enhanced by circulation anomalies associated with wave activity and supported by the BDC. In addition, the zonal TOC maximum was shifted poleward and westward in September 1988, covering the continental stations (particularly, Zhongshan and Davis) with higher TOC levels (Fig. 2b). SSW 1988 gave the largest contribution (blue dotted curves in Fig. S3) to the averaged anomalies in Fig. 6, while the anomalies of 2002 were near the climatological level (green dotted curves in Fig. S3). However, the anomaly amplitudes within the ±60-day time interval vary with a relatively monotonic seasonal change (Fig. 6) compared to strong peaks at the WH stations (Fig. 5). The propagation of Rossby waves tends to be directed poleward and upward at high latitudes (Rodas and Pulido, 2017; Domeisen et al., 2018), and this tends to cause the polar vortex and ozone hole to have a greater sensitivity to sudden dynamic disturbances than the midlatitude region outside the vortex. This would favor a more strongly pronounced SSW effect in the WH stations compared with the EH stations (Fig. 2b–2d). As noted in Section 3.1, the interaction of amplified waves with zonal flow at the polar vortex edge is mostly reflected in the variability of the low-ozone pattern inside the vortex and thus in the TOC anomalies at the WH stations.

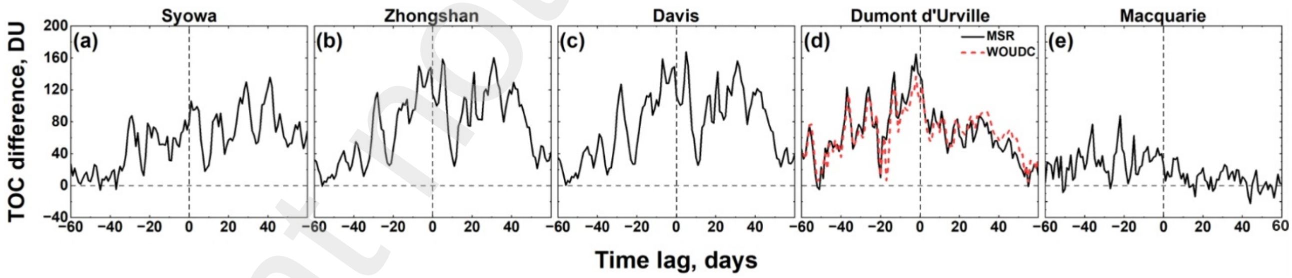

Figure 6. As in Fig. 5, but for the EH stations: (a) Syowa, (b) Zhongshan, (c) Davis, (d) Dumont-d'Urville and (e) Macquarie. Red line in (d) shows anomalies based on the WOUDC datasets for Dumont d'Urville.

The almost complete absence of negative anomalies in Fig. 6 confirms that the EH Antarctic stations in the SSW years are mainly influenced not by the ozone hole region, but by the zonal TOC maximum in the ozone collar region (Fig. 2b–2d). Anomalies at Macquarie are slightly elevated before day 0 at around 40 DU, and tend to decrease to climatological levels across the positive lags (Fig. 6e). This midlatitude station locates at the outer edge of the collar region and seems almost unresponsive to the SSW events (see also Fig. S3e).

Based on the results of Figs. S4 and S5, we estimated the average impact of the three SSW seasons on climatological changes in TOC relative to day 0 at each of the ten stations. Within a ±1 month lag, the relative difference between the TOC values averaged over all years in the period 1979–

2022 with SSW years and excluding SSW years (black and red curves in Figs. S4 and S5) is about 4–5%. Beyond a lag of ±1 month, the difference is usually even smaller, <3%. Thus, there is only a relatively small contribution of the three stratospheric warmings to the climatological TOC variation over the lag interval.

Figure 7a presents TOC anomalies averaged over three events and five stations of WH and five stations of EH (black and red curve, respectively). The properties of the anomaly variations in each hemisphere are clearly distinguished. On average, the EH stations have peak anomalies at about 110 DU near day 0. A time lag of up to +20 days is characteristic of increased positive anomalies at the WH stations reaching maximum at approximately 90 DU near day +5 (red and black curve in Fig. 7a). The anomalies at the WH and EH stations have almost identical tendencies and values between day +5 and day +15 (dashed vertical lines), and on the rest of the ±60 days, the former are several times smaller than the latter (black and red curves).

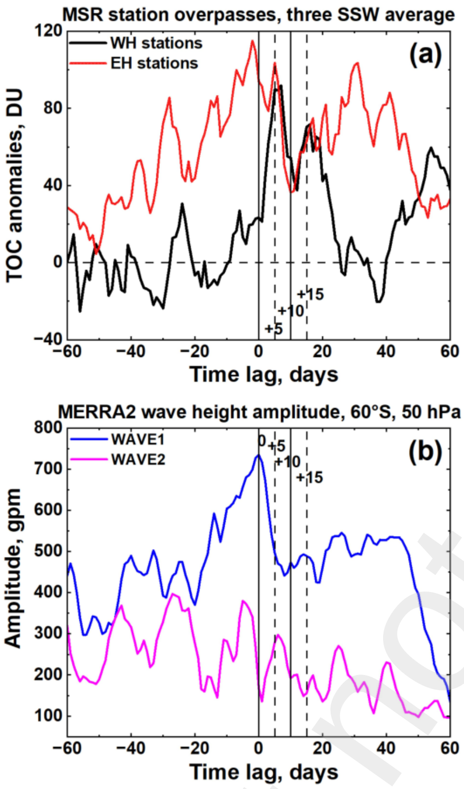

Figure. 7. (a) TOC anomalies averaging data for three SSW events separately for five Western Hemisphere stations (black curve) and five Eastern Hemisphere stations (red curve). The MSR-2 overpass data are used. (b) Wave 1 and wave 2 amplitudes in geopotential height (units m) at 60°S, 50 hPa using MERRA-2 data. The method of superimposed epochs with ±60-day time lag relative to the SSW central date was used. The time lags for day 0 and day +10 (day +5 and day +15) are indicated by solid (dashed) vertical lines.

A marked synchronous decrease in the anomaly amplitudes to a level of about 40 DU occurred to day +10 (between dashed vertical lines in Fig. 7a). This coincidence in time of the anomaly decline does not appear to be accidental, as each curve is an average of 15 data samples (3 events × 5 stations). From Fig. 5 and Fig. 6, it can be seen that a similar TOC minimum is present at four WH stations (AS, R, FV and U) and three EH stations (S, Z and D), respectively, near time lag +10 days.

Note that the close coincidence of the two curves between day +5 and day +15 with the common +10-day TOC minimum (Fig. 7a) implies their consistency in timing with respect to the central date of SSW (day 0). During the SSW main stage, the TOC maximum expanded both in latitude and longitude with increasing TOC not only at EH, but also at WH stations, as seen even from monthly means for September in the SSW years (Fig. 2b–2d). Therefore, ozone collar variability could contribute to synchronous anomaly variations at the WH and EH stations between day +5 and day +15 (Fig. 7a). Beyond this interval, a much higher level of TOC anomalies persists at the EH stations during the pre-SSW (negative time lag up to day –60) and post-SSW (approximately day +20 to day +50) periods (Fig. 7a). This difference may be due to generally opposite tendencies in stratospheric ozone depletion and accumulation occurring in zonally asymmetric regions during the ozone hole season. When averaging over the entire polar region, without dividing into stations WH and EH, a significant difference and relatively short-term proximity in the TOC anomalies in the zonally asymmetric pattern would not be detected.

The intervals of proximity and differences in the changes of TOC anomalies in WH and EH indicate the spatial dependence of the TOC response to dynamic variability. The alternation of higher and lower wave activity during SSW, diagnosed by wave amplitudes averaged over three events, is shown in Fig. 7b. Wave 1 has a significant peak amplitude of 720 gpm at day 0 and decreases by about 250 gpm during the +10-day lag (blue curve in Fig. 7b), similarly to the decreasing tendency in the TOC anomalies (Fig. 7a). It should be emphasized that both decreasing tendency and a common +10-day minimum in the TOC anomalies are timed to day 0. Since the maximum wave forcing coincides with the onset of SSW, and a wave 1 pulse was a cause of two of three analyzed events, this can explain a consistency in the maxima near day 0 in Fig. 7a and 7b. However, common +10-day minima in Fig. 7a are unexpected. Wave 1 exhibits similar changes between day +5 and day +15 (blue curve between dashed vertical lines in Fig. 7b), but they occur with a small difference in amplitude after day +5. Wave 2 weakens to low amplitude levels in this time interval (pink curve in Fig. 7b). Some of the discrepancy in the timing and magnitude of changes in TOC and wave 1 around day +10 can be explained by differences in the spatial scale and latitudes of the variables. TOC anomalies in Fig. 7a are averages over the local station data mainly within latitudes of 65°S–90°S (Table 1 and Fig. 1), while the wave amplitudes in Fig. 7b illustrate large-scale zonal anomalies at single latitude 60°S and single pressure level 50 hPa. The spatial dependence of differences in variability of waves and TOC requires a more detailed analysis and is beyond the scope of this work. The results of Fig. 7 generally indicate the role of wave 1 variability in the characteristic date and time scale of the strongest TOC modification in the three SSW events. Since wave 1 forms a zonally asymmetric accumulation of ozone (Sato et al., 2009; Gabriel et al., 2011), changes in wave 1 and TOC (Fig. 7b and 7a, respectively) may well be synchronized at the maximum of stratospheric warming and wave forcing due to increased ozone transport into the extended ozone collar region.

Wave 2 has a several times smaller amplitude (pink curve in Fig. 7b) and around the central date generally has variation in amplitude that is opposite to wave 1. The minimum amplitude of wave 2 on day 0 is about 150 gpm, five times smaller than wave 1 amplitude. Wave 2 appears to have a less pronounced effect on the ozone field perturbation than wave 1 when averaged over the three events.

All curves in Fig. 7 show quasi-periodic oscillations. It is known from theory and observations that the quasi-periodicity is characteristic of the winter stratosphere (Matsuno, 1971; Holton and Mass, 1976; Schoeberl, 1978; Yamazaki and Matthias, 2019; Tang et al., 2021). Preliminarily, TOC and wave amplitude anomalies vary with maximum spectral peaks between periods of 8 and 25 days (not shown), which may account for the observed variability (Fig. 7). The aspect of periodicity in the SH SSW events will be investigated in a separate work.

3.3 Changes in TOC field during SSW

Figure 8 shows daily TOC maps from the MSR-2 assimilated ozone fields with a 5-day step relative to the central date of SSW (columns −5 days, 0 day, +5 days, +10 days, and +15 days) for the three events. The time lag between −5 days and +15 days demonstrates the difference between the major SSW 2002 (middle panel) and the minor SSWs 1988 and 2019 (top and bottom panels). It can be seen that the ozone hole was separated into two parts on 24 September 2002 (day −5 in Fig. 8f) due to the splitting of the polar vortex (Varotsos, 2002; Charlton et al., 2005) under wave 2 forcing. Wave 2 briefly peaked in amplitude at about 700 gpm and quickly decreased to 200–300 gpm around day 0 (Fig. 9b, dashed curve). As inferred from MERRA-2 for 60°S and 50 hPa, in all events since day 0, wave 1 appears to have been the main driver of the stratospheric dynamics over Antarctica (solid curves in Fig. 9).

The joint effect of intense, almost equal-amplitude waves 1–2 near SSW onset (Fig. 9b) led to a strong deformation of the collar region in SSW 2002 (Fig. 8f–8h). The deformation was accompanied by the replacement of low TOC by a high TOC over part of the polar region including the pole itself (Fig. 8f and 8g). Ozone-rich air masses in the SH polar region of such an unusual shape and location are observed quite rarely and did not appear in 1988 and 2019 (top and bottom panels in Fig. 8). The result of this poleward intrusion was that, according to Fig. 5a, the TOC anomaly at Amundsen-Scott station near day 0 was the highest among WH stations (Fig. 5). At the same time, warming of the polar cap was observed according to the zonal mean temperature (Newman and Nash, 2005).

As the high-TOC area turned eastward in SSW 2002, the WH stations R, FV and U were under its influence later, from day +5 (Fig. 8h–8j). This is seen from times series in Fig. S2c–S2e (green dotted curves). Among the three events, the WH stations (excluding Neumayer) were under the highest TOC area near the SSW onset only in 2002 (Fig. 8). So, the time delay of maximum TOC anomalies in Fig. 5 was mainly determined by the contribution of SSW 2002. Neumayer was predominantly under the low TOC area in all events (N in Fig. 8), and the averaged time series did not show a significant peak during SSW (Fig. 5b).

Zonal TOC asymmetry during SSW 1988 and 2019 (top and bottom panels in Fig. 8) compared to SSW 2002 (middle panel) was closer to the climatological one in Fig. 2a with an approximately ring-shaped ozone collar region. In the absence of a strong pulse of wave 2, SSWs 1988 and 2019 developed under the dominant action of wave 1 (dashed and solid curves in Fig. 9a and 9c). Near the SSW onset, these vortex displacement events were characterized by east–west zonal asymmetry in TOC (Fig. 8a–8c, 8k–8m). The maximum amplitude of wave 1 was much larger in 1988 than in 2019, 920 gpm and 740 gpm, respectively (solid curves in Fig 9a and 9c). Thus, the collar region came further poleward beyond the edge of the continent covering the EH stations with the higher TOC levels (Fig. 8a–8c) and causing the highest TOC maxima here near day 0 in 1988 (blue dotted curves in Fig. S3). Smaller TOC maxima near day 0 were observed at stations S, Z and D in 2019 (pink dotted curves in Fig. S3a–S3c).

Overall, there are similar wave 1 effects for 1988 and 2019 in both zonal TOC asymmetry patterns and TOC increases at the EH stations. However, anticorrelated TOC oscillations around the central date in 2002 (green dotted curves in Fig. S3a–S3c) compensated to some degree these effects when averaging TOC over the three SSWs (Fig. 6). This may account for the lack of strong positive anomalies that stand out sharply near day 0, as observed at the WH stations (Fig. 5). That is, in this comparison, we focus on the differences and similarities not only of each of the SSWs (Shen et al., 2020; Roy et al., 2022; Mitra and Guharay, 2024), but also of their effects on TOC at stations of WH and EH. Note that the relationship between the wave amplitudes in the three SSWs at 50 hPa, or 20 km altitude (Fig. 9), is somewhat different from the relationship at 10 hPa (32 km) in Roy et al. (2022). When analyzing variations in total ozone, we use the 50 hPa level, which is near the maximum of stratospheric ozone in its vertical profile (McPeters et al., 2007; Wei et al., 2010).

Returning to the time series of the amplitude of wave 1 in Fig. 9 (solid curve), it is worth noting that it decreased between day 0 and day +10 in all events (in Fig. 9). This is clearly reflected in average tendency in Fig. 7b (blue curve). Weakening of wave 1 means a decrease in both the displacement of the vortex relative to the pole and the zonal TOC asymmetry with a simultaneous increase in vortex strength, or a partial vortex recovery and subsequent cooling (Hitchcock et al., 2013; Roy et al., 2022).

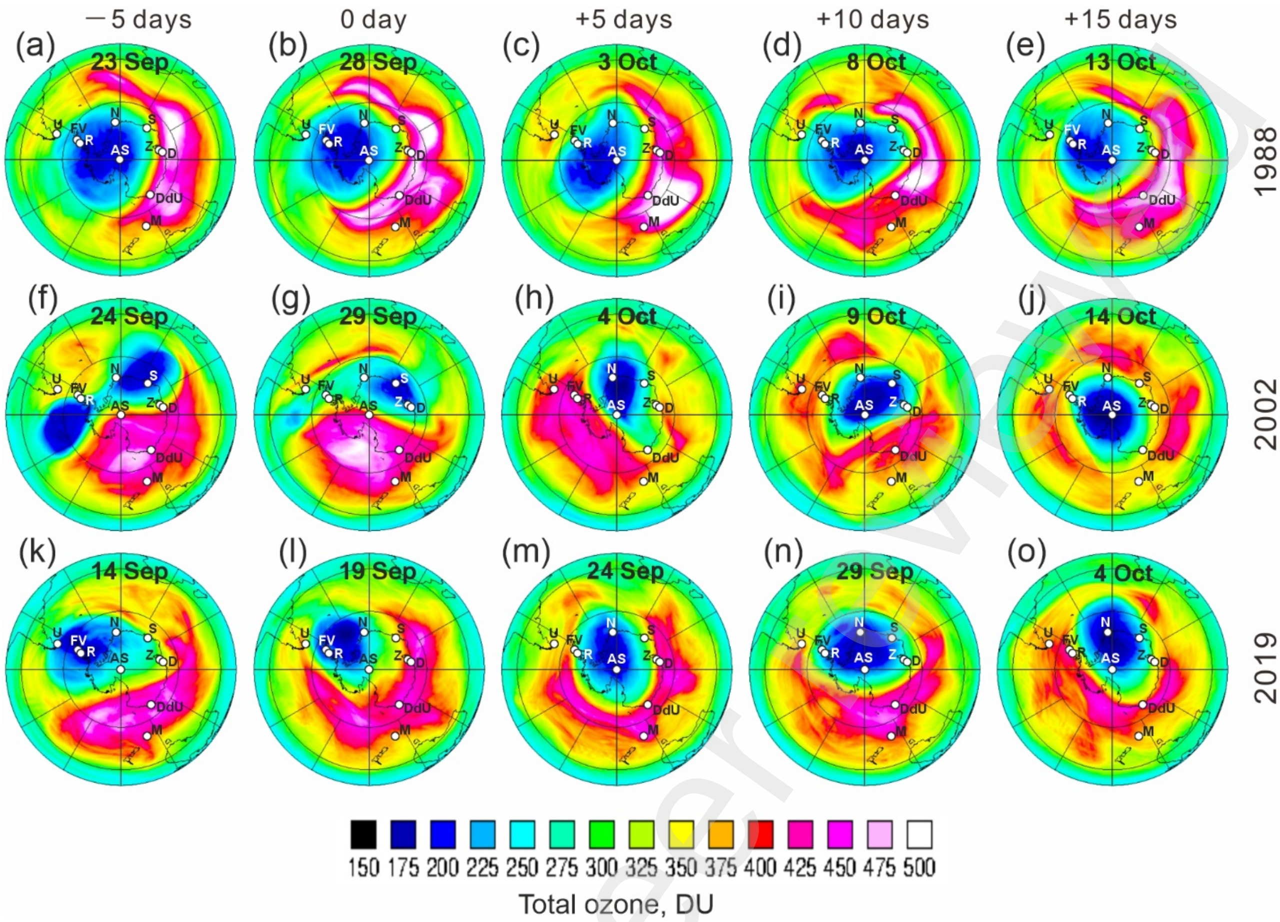

Figure 8. Maps of TOC for SSW periods in (top panel) 1988, (middle panel) 2002, and (bottom panel) 2019. The five columns are aligned relative to the central date (day 0) of SSW with a 5-day step from −5 days to +15 days. The latitude−longitude grid, location and designation of research stations correspond to those shown in Fig. 2. MSR-2 data are used.

This tendency led to an expansion of the low-ozone area on day +10 relative to days 0 and +5, to its coverage of more stations (blue at about 200–225 DU in respective columns in Fig. 8) and to the appearance of a +10-day minimum TOC anomalies when averaging over 15 time series in both WH and EH (Fig. 7a).

Because the amplitude of wave 1 decreased after reaching peak level during SSW onset, along with decreasing vortex displacement, the TOC fields became more zonally symmetric in all events (Fig. 8, columns +10 days and +15 days).

Figures 8 and 9, based on assimilated satellite ozone fields (MSR-2) and wave amplitudes (MERRA-2), respectively, show specific manifestations of wave–zonal flow interactions (Holton and Mass, 1976) in total ozone (Bahramvash Shams et al., 2022). The wave 1 and wave 2 effects in September of the SH SSW years are changing (1) the size and shape of the ozone hole and collar regions and (2) TOC levels inside and outside the polar vortex during the SSW events, inevitably affecting local observations under the perturbed ozone field.

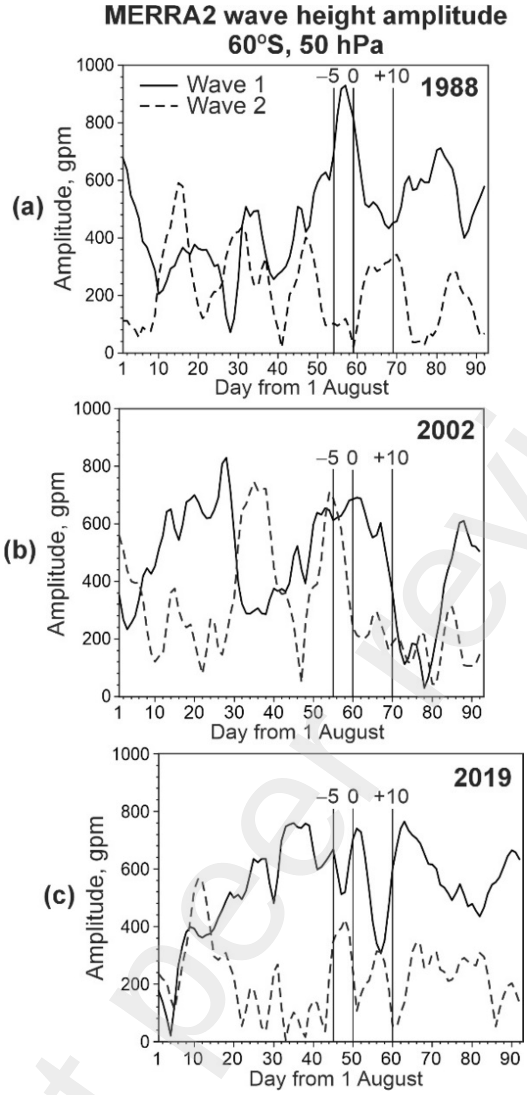

Figure 9. Amplitudes of wave 1 and wave 2 in the geopotential height in August–October (a) 1988, (b) 2002 and (c) 2019. For ease of comparison with changes in the TOC fields near the SSW central date in Fig. 8, vertical lines indicate time lags of –5, 0 and +10 days, and horizontal axes are aligned to day 0.

4 Discussion

We examined the evolution of three SSW events basing on the TOC time series over ten stations of Antarctica and sub-Antarctic region, TOC fields in the SH, and amplitudes of wave 1 and wave 2 in the polar stratosphere. The SSW events of 1988, 2002, and 2019 have been comprehensively studied over the past decades, both individually and comparatively (Section 1). Using mostly zonal mean or area averaged data, either all of these events (Shen et al., 2020; Milinevsky et al., 2020; Roy et al., 2022) or two of them (Grytsai et al., 2008; Kozubek et al., 2020; Klekociuk et al., 2021; Ma et al., 2022; Mitra and Guharay, 2024; Veenus and Das, 2024) were compared. Because of the uniqueness of major warmings in the SH, some studies included events with less dramatic changes in stratospheric conditions and used less stringent criteria for stratospheric warming. Vincent et al. (2022) reported extended statistics of 37 August–October events that occurred from 1995 to 2019. The warmings were identified by westerly weakening at 60°S and corresponding increase in the polar cap temperature at the 10 hPa ranged from 3 to 28 K. In terms of poleward temperature gradient reversal at 10 hPa, 16 weak polar vortex events were analyzed in (Shen et al., 2022). Among other properties, studies have consistently emphasized the dominance of wave 1, episodic intensifications of wave amplitudes, total ozone increase and its zonal asymmetry over Antarctica during SSWs.

Our analysis focuses on the three most prominent events, includes local ozone data, uses a superimposed epoch method with a ±60-day time lag relative to the central date of SSW, and applies a regional division of the time series. This approach reveals new features of the zonally asymmetric response of TOC to SSW. With all the individuality of each of the three SH SSW events, we tried to identify common features, which are characteristic either of all events or, according to our division, of their impact on TOC at the stations of the WH and EH. Using a lagged composite and averaging over three events and over five stations in both WN and EH, we found (i) an effect of zonal TOC asymmetry during SSW evolution with weaker (stronger) positive TOC anomalies in WH (EH) compared to the climatology, (ii) a difference in the timing of response maxima (day 0 in EH and day +5 in WH), and (iii) joint minimum of TOC anomalies in WH and EH near time lag of +10 days, associated with a decrease in the wave 1amplitude.

Zonal asymmetry in the Antarctic stratosphere is formed due to the interaction of wave 1 with the cyclonic zonal flow (polar vortex), which becomes more displaced off the pole under more intense wave forcing (Waugh and Randel, 1999). With a corresponding asymmetry in ozone (Section 1), the spatially distributed stations of the Antarctic region (Fig. 1) are in very different conditions of the average TOC level both climatologically and in individual events (Figs. 2–6). The main components of the uneven spatial distribution of ozone are the areas inside and outside the vortex, the ozone hole and the ozone collar (Mariotti et al., 2000; Pazmiño et al., 2005; Grytsai et al., 2007; Agosta and Canziani, 2010).

Pazmiño et al. (2005) classified ozone data as a function of the position of the stations with respect to the polar vortex (inside, at the edge of, and outside the vortex). They included in the analysis the two midlatitude (Ushuaia and Comodoro Rivadavia) and three Antarctic (Marambio, Dumont d'Urville and South Pole) stations. The best correlation between total ozone and vortex metrics was found at 550 K isentropic surface. This is close to the level of 50 hPa, or 20 km, which corresponds to the maximum stratospheric ozone amount in its vertical profile (McPeters et al., 2007; Wei et al., 2010) and which we have chosen to examine the association between wave amplitudes (Fig. 7b and Fig. 9) and TOC (Fig. 8). Similar to our result (i), the authors showed a clear difference in total ozone observed between inside and outside situations. The variability in displacements of the vortex and ozone-depleted region determined the evolution of total ozone at the stations. If it was close to 350 DU outside the vortex, then the minimum levels of about 120 DU were measured inside the vortex (Pazmiño et al., 2005).

To better highlight the SSW effects, we consider these dynamic processes relative to the central date of the events. We show in detail in Section 3.3 and Fig. 8, how the elements of the perturbed, zonally asymmetric TOC field migrate in latitude and longitude and in time relative to day 0. There is a continuously change the position of low and high levels of TOC over the Antarctic and sub-Antarctic stations. Considering the average tendencies, the zonal asymmetry was manifested in the TOC anomaly maxima of 110 DU (EH) and 90 DU (WH) near day 0 (Fig. 7a). In comparison, a close estimate was obtained for TOC anomalies averaged over 20 major NH SSW events, which were enhanced up to 90 DU after the SSW onset (Hocke et al., 2015).

The impact of ozone-depleted air mass occurrences on ultraviolet (UV) radiation was estimated. From the UV measurements, an average percentage UV increase of 68% at Ushuaia and of 47% at Marambio affected increases of the erythemal UV dose (Pazmiño et al., 2005). We demonstrate the spatial extent and position of the low-ozone region in the climatology (Fig. 2) and in some cases, when the ozone hole may pass over densely populated areas of South America (Fig. 8k). Researchers at dozens of Antarctic stations may be more frequently exposed to elevated erythemal UV doses during ozone hole season. However, it is worth noting that higher levels of UV radiation are observed under the strong and cold vortex with significant ozone depletion, than under the warmer stratosphere during a SSW (Klekociuk et al., 2021).

Differences between the WH and EH stations in the timing of the maximum TOC response in result (ii) is explained by the eastward shift of the zonal TOC maximum. In September of the SSW years, the collar region becomes latitudinally and longitudinally much more extended than in the climatology (Fig. 2) with an eastward migration of the higher TOC levels during SSW development (Fig. 8). Since wave 1 is responsible for the zonal asymmetry, its eastward-migrating component is able to influence changes in the TOC field. Eastward-propagating planetary wave 1 exists in the polar stratosphere of both hemispheres (Tang et al., 2021) and is observed in the TOC variability at 65°S, particularly, in September (Grytsai et al., 2005). Indeed, eastward phase speeds of upward and poleward propagating waves from the troposphere appear favored (Domeisen et al., 2018). The zonal TOC maximum is climatologically located in the EH, and the amplification of eastward-propagating wave 1 causes advancing of the zonal TOC maximum to the east into WH. This tendency is clearly visible from the sequence the maps in Fig. 8 (columns –5 days, 0 day and +5 days) in all three events, qualitatively explaining the 5-day difference between the TOC maxima in WH and EH in Fig. 7a.

Fairly synchronous changes in anomalies of WH and EH between day +5 and day +15 and their common minimum near day +10 (red and black curves in Fig. 7a) in the result (iii) can be attributed to the alternation of strengthening and weakening of planetary waves during the SSW event warming (Fig. 7b). When intense planetary waves are propagated from the troposphere upward, the strong stratospheric westerly is weakened and no longer acts as a barrier for wave propagation (Charney and Drazin, 1961; Matsuno, 1971). The wave amplitude peak is accompanied by the strongest deceleration (or even reversal) of the zonal wind, and planetary waves are again inhibited from propagating further upward resulting in a reduction of their amplitude (Matsuno, 1971). After the velocity minimum near the central date of SSW, increasing westerly circulation is usually observed in the polar stratospheres (Allen et al., 2003; Charlton and Polvany, 2007; Oehrlein et al., 2020; Roy et al., 2022), indicating the polar vortex recovery (Hitchcock and Shepherd, 2013; Baldwin et al., 2021).

Common anomaly weakening around day +10 at the EH and WH stations (both curves in Fig. 7a) is obviously associated with reduced wave activity due to interaction with decelerated zonal flow. Veenus and Das (2024) show that wave driving, and poleward and downward ozone transport were intensified before and during SSW 2002 and 2019 and greatly reduced from the central date to day +10 due to the changed atmospheric wind conditions hindering wave propagation. A decrease of wave 1 amplitude in Fig. 7b after day 0 corresponds to an increase in zonal wind at 60°S, 50 hPa by about 10 m s^{-1} (not shown) and a TOC decrease by 50 DU (WH) and 70 DU (EH) (Section 3.2, Fig. 7a).

Note that, in contrast to the middle stratosphere at 10 hPa, the zonal wind in the lower stratosphere at 50 hPa did not reverse in 2002 and only decreased to 15 m s^{-1}; the minimum velocity near day 0 was of 35 m s^{-1} in 1988 and 2019 (not shown). Nevertheless, the dynamical impacts following a wind deceleration to some nonzero values are essentially equivalent to the impacts of a complete wind reversal (Butler et al., 2015) and are able to modify wave activity. As a result, wave–zonal flow interaction during highly altered dynamics of SSWs eventually leads to ozone variations (Bahramvash Shams et al., 2022).

In zonal means, ozone anomalies over the Arctic are positive within one–three months after the SSW onset (de la Camara et al., 2018; Bahramvash Shams et al., 2022; Shi et al., 2024b). This is in general agreement with lagged anomaly tendencies in Fig. 7a, however, the latter reveal a dependence on the zonal asymmetry of TOC. The TOC anomalies at the EH stations are larger in magnitude and, particularly, become anticorrelated to those at the WH stations after about day +20 (red and black curves in Fig. 7a). The wave enhancement, TOC anomaly increases and large disturbances of the TOC field during SSW (Fig. 7 and Fig. 8) are accompanied by the increased ozone transport between the tropics and polar region due to BDC (Weber et al., 2011; Butchart, 2014; de la Cámara et al., 2018; Veenus and Das, 2024). As the enhanced ozone transport is zonally asymmetric (Sato et al., 2009; Gabriel et al., 2011), its influence is most (less) noticeable in the ozone accumulation over the collar region (ozone hole area) (Fig. 2b–2d). Modulated by the coupled wave–BDC dynamics during SSW, extension of collar region into WH may contribute to synchronization of anomalies between day +5 and day +15 (Fig. 7a). Outside this interval, weakened wave activity does not provide sufficient penetration of collar region into WH, which disrupts synchronization between WH and EH. The anomalies at the EH stations remain larger being mostly influenced by the ozone collar region (red curve in Fig. 7a). In contrast, the WH stations fall under the zonal TOC minimum associated with the depleted ozone in the ozone hole area (Fig. 2), which contributes less to the positive TOC anomalies (black curve in Fig. 7a). However, the details of assumed coupled dynamics of waves, circulation, and ozone still require further analysis considering the effects of asymmetry in the Antarctic stratosphere.

In terms of planetary wave propagation theory, waves may interact with the stratospheric zonal wind to produce a vacillation regime, in which both the waves and the mean flow oscillate on a 10–20-day time scale (Matsuno, 1971; Holton and Mass, 1976). Wave amplification may also be irregularly spaced with a periodicity of approximately 1–3 week, as in the SSW 2002 (Newman and Nash, 2005). A well-known 5-, 10- and 16-day waves (Ma et al., 2022; Yamazaki and Matthias, 2019; Tang et al., 2021) are frequently observed in the stratosphere. Sjoberg and Birner (2014) show in their model that the stratosphere has a preferred wave forcing time scale associated with SSW with wave pulse duration on the order of 10 days. A stratospheric 10-day wave 1 dominated in SH in September during 2007–2019 (Huang et al., 2021) and, particularly, during the SSW onset in September 2019 (Wang et al., 2021).

In our results, wave amplitudes in Fig. 7b and TOC in Fig. 7a show quasi-periodic variations. A close wave–ozone coupling is especially clearly seen in the consistent change in wave 1 and TOC from day 0 to day +10 (between solid vertical lines in Fig. 7). Judging from Fig. 7, oscillations in the range of periods of 9–25-days may be involved to observed variability. The results of Fig. 7 suggest that, using larger statistics of the SSW events (e.g. Vincent et al., 2022; Shen et al., 2022; Hocke et al., 2015), it would be possible to more clearly and fully describe the periodicity of the wave–ozone interaction during the SSW life cycle.

5 Conclusions

Our main results are based on the MSR-2 and MERRA-2 reanalyses and the comparison of local TOC time series, TOC fields and wave amplitudes in the three SH SSW events of 1988, 2002 and 2019. The analysis is made using the method of superimposed epochs with ±60-day time lag relative to the central date of SSWs and including a regional division of the time series. With this approach, new features of the zonally asymmetric response of TOC to SSW has been revealed. We identified distinct and common TOC tendencies that are characteristic, according to our separation, of SSW impacts over the stations of WH and EH. Using the lagged composite and averaging the three events and five station time series in both WN and EH, we found (i) an effect of zonal TOC asymmetry during SSW evolution with smaller (larger) TOC anomalies in the WH (EH) compared to the climatology, (ii) a difference in timing of the response maxima (day 0 in EH and day +5 in WH), and (iii) synchronized anomalies between day +5 and day +15 with a common TOC minimum near a time lag of +10 days, associated with a decrease in the amplitude of wave 1. This timing in (ii) and (iii) relative to the central date of SSWs appears robust as it represents a total of 30 data samples (three events and ten stations), and appears driven by the characteristics of the prevailing large-scale waves.

Climatology shows that the quasi-stationary zonal minimum (WH) and maximum (EH) of TOC determine the mean levels and range of changes of TOC in its annual cycle. Different tendencies in stratospheric ozone depletion (ozone hole region) and ozone accumulation (ozone collar region) impose differences in the responses of TOC anomalies to SSW in WH (weaker) and EH (stronger). The local TOC time series recorded in the Antarctic and sub-Antarctic regions appear to be depended on the latitude and longitude of the stations.

The asymmetric TOC pattern is formed due to wave 1 and is contributed by polar vortex displacement off the pole and zonally asymmetric BDC. The observed rapid decrease in wave 1 amplitude after the SSW central date likely cause large-scale change in the wave–zonal flow interaction and ozone transport in the Antarctic region. Presumably, this could, within a relatively short interval, both synchronize in time TOC anomalies in zonally asymmetric regions and equalize their magnitude through the expansion of the collar region into WH. The time scale of this process in our composites is within 10–15 days and, it should be emphasized, is tied to the central date of SSW. It is assumed that extension of collar region into WH, modulated by the coupled wave–BDC dynamics during SSW, may contribute to synchronization of anomalies in WH and EH. Weakened wave activity after the main phase of SSW does not provide sufficient penetration of collar region into WH, which disrupts synchronization. The anomalies at the EH stations remain larger being mostly influenced by the ozone collar region, whereas the WH stations fall more often under the ozone depleted area, which contributes less to the positive TOC anomalies. The observed quasi-periodic variations in TOC and waves are similar to the typical periodicity of the stratospheric oscillations known from theory and observations for the winter season in general and for SSW events in particular. In this regard, the role of periodicity in the development of SSW needs to be better elucidated.

Author Contributions: Conceptualization, A.G., A.B. and G.M.; methodology, A.G. and G.M.; data acquisition, R.Y, O.E., A.B., O.P. and X.W.; software and related figures, A.G., R.Y., O.E., O.I., and Y.S.; validation, R.Y., O.E., A.B. and G.M.; investigation and interpretation, A.G., O.P., A.K., G.M., and X.W.; writing-original draft preparation, A.G., R.Y., O.E., A.K. and G.M.; writing-review and editing, A.G., O.E., A.K., Y.S., G.M., and A.G.; visualization, R.Y., A.G., O.E., and O.I.; supervision, G.M. and X.W.; project administration, A.G. and G.M. Each author contributed to the interpretation and discussion of the results and edited the manuscript. All authors have read and agreed to the published version of the manuscript.

Funding: This research has been supported in part by the National Antarctic Scientific Center of Ukraine (Project Number: NASC–2024) and the Jilin University (Grant Number: G2023129024L).

Acknowledgments. This work was provided under support by the College of Physics, International Center of Future Science, Jilin University, China. This research contributed to Project 4293 of the Australian Antarctic Program, and to the National Antarctic Scientific Center of Ukraine research objectives. MSR-2 reanalysis data were provided by the Tropospheric Emission Monitoring Internet Service (TEMIS), from their website at https://temis.nl/protocols/o3field/overpass_msr2.php.

Conflicts of Interest: The authors declare no conflict of interest.

References

Allen, D.R., Bevilacqua, R.M., Nedoluha, G.E., Randall, C.E., Manney, G.L. (2003). Unusual stratospheric transport and mixing during the 2002 Antarctic winter. Geophys. Res. Lett., 30, 1599. doi:10.1029/2003GL017117.

Agosta, E.A., Canziani, P.O. (2010). Interannual variations in the zonal asymmetry of the subpolar latitudes total ozone column during the austral spring. Geoacta, 35, 1–16. https://revistas.unlp.edu.ar/geoacta/article/view/13601.

Bahramvash Shams, S., Walden, V.P., Hannigan, J.W., Randel, W. J., Petropavlovskikh, I.V., Butler, A.H., and de la Cámara, A. (2022). Analyzing ozone variations and uncertainties at high latitudes during sudden stratospheric warming events using MERRA-2, Atmos. Chem. Phys., 22, 5435–5458, https://doi.org/10.5194/acp-22-5435-2022.

Baldwin, M.P., Ayarzagüena, B., Birner, T., Butchart, N., Butler, A. H., Charlton-Perez, A. J., Domeisen, D.I.V., Garfinkel, C.I., Garny, H., Gerber, E.P., Hegglin, M.I., Langematz, U., Pedatella, N.M. (2021). Sudden stratospheric warmings. Reviews of Geophysics, 59, e2020RG000708. https://doi.org/10.1029/2020RG000708.

Baldwin, M., Hirooka, T., O'Neill, A., Yoden, S. (2003). Major stratospheric warming in the Southern Hemisphere in 2002: Dynamical aspects of the ozone hole split. SPARC Newsletter, 20, 24–26. https://www.atmosp.physics.utoronto.ca/SPARC/News20/20_Baldwin.html.

Butchart, N. (2014) The Brewer-Dobson circulation. Rev. Geophys., 52, 157–184. https://doi.org/10.1002/2013RG000448.

Butler, A.H., Seidel, D.J., Hardiman, S.C., Butchart, N., Birner, T., Match, A. (2015). Defining sudden stratospheric warmings. Bull. Amer. Meteorol. Soc., 96, 1913–1928. https://doi.org/10.1175/BAMS-D-13-00173.1.

Chandran, A., Collins, R. L. (2014). Stratospheric sudden warming effects on winds and temperature in the middle atmosphere at middle and low latitudes: a study using WACCM, Ann. Geophys., 32, 859–874, https://doi.org/10.5194/angeo-32-859-2014.

Charlton, A.J., O'Neill, A., Lahoz, W.A., Berrisford, P. (2005). The splitting of the stratospheric polar vortex in the Southern Hemisphere, September 2002: Dynamical evolution. J. Atmos. Sci., 62, 590–602. https://doi.org/10.1175/JAS-3318.1.

Charlton, A. J., Polvani, L. M. (2007). A new look at stratospheric sudden warmings. Part I: Climatology and modeling benchmarks. J. Clim., 20, 449–469, https://doi.org/10.1175/JCLI3996.1.

Charney, J.G., Drazin, P.G. (1961). Propagation of planetary-scale disturbances from the lower into the upper atmosphere. J. Geophys. Res., 66, 83–109. https://doi.org/10.1029/JZ066i001p00083.

de la Cámara, A., Abalos, M., Hitchcock, P. (2018). Changes in stratospheric transport and mixing during sudden stratospheric warmings. Journal of Geophysical Research: Atmospheres, 123, 3356–3373. https://doi.org/10.1002/2017JD028007.

Domeisen, D.I.V., Butler, A.H. (2020). Stratospheric drivers of extreme events at the Earth's surface. Commun Earth Environ 1, 59. https://doi.org/10.1038/s43247-020-00060-z.

Domeisen, D. I. V., Martius, O., Jiménez-Esteve, B. (2018). Rossby wave propagation into the Northern Hemisphere stratosphere: The role of zonal phase speed. Geophys. Res. Lett., 45, 2064–2071. https://doi.org/10.1002/2017GL076886.

Eswaraiah, S., Seo, K., Kumar, K.N., Koval, A.V., Ratnam, M.V., Mengist, C.K., Chalapathi, G.V., Liu, H., Kwak, Y., Merzlyakov, E., Jacobi, C., Kim, Y., Rao, S.V., Mitchell, N.J. (2023). Intriguing aspects of polar-to-tropical mesospheric teleconnections during the 2018 SSW: A meteor radar network study. Atmosphere, 14(8), 1302. https://doi.org/10.3390/atmos14081302.

Farman, J.C. (1987). Recent measurements of total ozone at British Antarctic Survey stations. Philosophical Transactions of the Royal Society of London. Series A, Mathematical and Physical Sciences, 323, 629-644. https://doi.org/10.1098/rsta.1987.0110.

Fioletov, V.E.; Shepherd, T.G. (2003). Seasonal persistence of midlatitude total ozone anomalies. Geophys. Res. Lett., 30, 1417. https://doi.org/10.1029/2002GL016739.

Gabriel, A., Körnich, H., Lossow, S., Peters, D.H.W., Urban, J., Murtagh, D. (2011). Zonal asymmetries in middle atmospheric ozone and water vapour derived from Odin satellite data 2001–2010. Atmos. Chem. Phys., 11, 9865–9885. https://doi.org/10.5194/acp-11-9865-2011.

Gelaro, R., McCarty, W., Suárez, M.J., Todling, R., Molod, A., Takacs, L., Randles, C.A., Darmenov, A., Bosilovich, M.G., Reichle, R., Wargan, K., Coy, L., Cullather, R., Draper, C., Akella, S., Buchard, V., Conaty, A., Silva, A.M. da, Gu, W., Kim, G.K., Koster, R., Lucchesi, R., Merkova, D., Nielsen, J. E., Partyka, G., Pawson, S., Putman, W., Rienecker, M., Schubert, S.D., Sienkiewicz, M., Zhao, B. The Modern-Era Retrospective Analysis for Research and Applications, Version 2 (MERRA-2). J. Clim., 30, 5419–5454. https://doi.org/10.1175/JCLI-D-16-0758.1.

Grytsai, A. V., Evtushevsky, O. M., Milinevsky, G. P. (2008). Anomalous quasi-stationary planetary waves over the Antarctic region in 1988 and 2002. Annales Geophysicae, 26, 1101–1108. https://doi.org/10.5194/angeo-26-1101-2008.

Grytsai, A.V., Evtushevsky, O.M., Agapitov, O.V., Klekociuk, A.R., Milinevsky, G.P. (2007). Structure and long-term change in the zonal asymmetry in Antarctic total ozone during spring. Ann. Geophys., 25, 361–374. https://doi.org/10.5194/angeo-25-361-2007.

Grytsai, A., Grytsai, Z., Evtushevsky, A., Milinevsky, G., Leonov, N. (2005) Zonal wave numbers 1–5 in planetary waves from the TOMS total ozone at 65°S. Ann. Geophys., 23, 1–9.

Grytsai, A., Klekociuk, A., Milinevsky, G., Evtushevsky, O., Stone, K. (2017). Evolution of the eastward shift in the quasi-stationary minimum of the Antarctic total ozone column. Atmospheric Chemistry and Physics, 17, 1741–1758. https://doi.org/10.5194/acp-17-1741-2017.

Hassler, B., Bodeker, G.E., Solomon, S., Young, P.J. (2011). Changes in the polar vortex: Effects on Antarctic total ozone observations at various stations. Geophys. Res. Lett., 38, L01805. doi:10.1029/2010GL045542.

Hendrick, F., Pommereau, J.-P., Goutail, F., Evans, R. D., Ionov, D., Pazmino, A., Kyrö, E., Held, G., Eriksen, P., Dorokhov, V., Gil, M., and Van Roozendael, M. (2011). NDACC/SAOZ UV-visible total ozone measurements: improved retrieval and comparison with correlative ground-based and satellite observations, Atmos. Chem. Phys., 11, 5975–5995, https://doi.org/10.5194/acp-11-5975-2011.

Hirota, I., Kuroi, K., & Shiotani, M. (1990). Midwinter warmings in the southern hemisphere stratosphere in 1988. Quarterly Journal of the Royal Meteorological Society, 116(494), 929–941. https://doi.org/10.1002/qj.49711649407.

Hitchcock, P., Shepherd, T.G. (2013). Zonal–mean dynamics of extended recoveries from stratospheric sudden warmings. J. Atmos. Sci., 70, 688–707. https://doi.org/10.1175/JAS-D-12-0111.1.

Hitchcock P., Shepherd T.G., Manney G.L. (2013). Statistical characterization of Arctic polar-night jet oscillation events. J. Clim, 26, 2096–2116. https://doi.org/10.1175/JCLI-D-12-00202.1.

Hocke, K., Lainer, M., Schanz, A. (2015). Composite analysis of a major sudden stratospheric warming. Ann. Geophys., 33, 783–788. https://doi.org/10.5194/angeo-33-783-2015.

Huang, C., Li, W., Zhang, S., Chen, G., Huang, K., Gong, Y. (2021). Investigation of dominant traveling 10-day wave components using long-term MERRA-2 database. Earth Planets Space, 73, 85. https://doi.org/10.1186/s40623-021-01410-7.

Ialongo, I., Sofieva, V., Kalakoski, N., Tamminen, J., Kyrölä, E. (2012). Ozone zonal asymmetry and planetary wave characterization during Antarctic spring. Atmos. Chem. Phys., 12, 2603–2614. https://doi.org/10.5194/acp-12-2603-2012.

Jucker, M., Reichler, T., Waugh, D.W. (2021). How frequent are Antarctic sudden stratospheric warmings in present and future climate? Geophys. Res. Lett., 48, e2021GL093215. https://doi.org/10.1029/2021GL093215.

Kalnay, E., Kanamitsu, M., Kistler, R., Collins, W., Deaven, D., Gandin, L., Iredell, M., Saha, S., White, G., Woollen, J., Zhu, Y., Chelliah, M., Ebisuzaki, W., Higgins, W., Janowiak, J., Mo, K.-C., Ropelewski, C., Wang, J., Leetmaa, A., Reynolds, R., Jenne, R., Joseph, D. (1996). The NCEP–NCAR 40-year reanalysis project. Bull Am Meteorol Soc 77:1057–1072. https://doi.org/10.1175/1520-0477(1996)077%3C0437:TNYRP%3E2.0.CO;2.

Kanzawa, H., Kawaguchi, S. (1989). Large stratospheric sudden warming in Antarctic late winter and shallow ozone hole in 1988. Geophysical Research Letters, 17, 77–80. https://doi.org/10.1029/GL017i001p00077.

Klekociuk, A.R., Matthew, A.H., Tully, B., Krummel, P.B., Henderson, S.I., Smale, D., Querel, R., Nichol, S., Alexander, S.P., Fraser, P.J., Nedoluha G. (2021). The Antarctic ozone hole during 2018 and 2019. Journal of Southern Hemisphere Earth Systems Science, 71, 66–91. https://doi.org/10.1071/ES20010.

Kozubek, M., Lastovicka, J., Krizan, P. (2020). Comparison of key characteristics of remarkable SSW events in the Southern and Northern Hemisphere. Atmosphere, 11(10), 1063. https://doi.org/10.3390/atmos11101063.

Lim, E., Hendon, H., Butler, A., Thompson, D., Lawrence, Z., Scaife, A., Shepherd, T., Polichtchouk, I., Nakamura, H., Kobayashi, C., Comer, R., Coy, L., Dowdy, A., Garreaud, R., Newman, P., Wang, G. (2021). The 2019 Southern Hemisphere stratospheric polar vortex weakening and its impacts. Bulletin of the American Meteorological Society, 102, E1150–E1171. https://doi.org/10.1175/BAMS-D-20-0112.1.

Ma, Z., Gong, Y., Zhang, S., Xiao, Q., Huang, C., and Huang, K. (2022). A new methodology for measuring traveling quasi-5-day oscillations during sudden stratospheric warming events based on satellite observations, Atmos. Chem. Phys., 22, 13725–13737. https://doi.org/10.5194/acp-22-13725-2022.

Malanca, F.E., Canziani, P.O., Argüello, G.A. (2005). Trends evolution of ozone between 1980 and 2000 at midlatitudes over the Southern Hemisphere: Decadal differences in trends, J. Geophys. Res., 110, D05102, doi:10.1029/2004JD004977.

Mariotti, A., Mechoso, C. R., Legras, B., and Daniel, V. The evolution of the ozone "collar" in the Antarctic lower stratosphere during early August 1994, J. Atmos. Sci., 57, 402–414, 2000. https://doi.org/10.1175/1520-0469(2000)057<0402:TEOTOC>2.0.CO;2.

Matsuno, T. (1971). A dynamical model of the stratospheric sudden warming. J. Atmos. Sci., 28, 1479–1494. https://doi.org/10.1175/1520-0469(1971)028<1479:ADMOTS>2.0.CO;2.

McPeters, R.D., Labow, G.J., Logan, J.A. (2007). Ozone climatological profiles for satellite retrieval algorithms. J. Geophys. Res., 112, D05308. doi:10.1029/2005JD006823.

Milinevsky, G., Evtushevsky, O., Klekociuk, A., Wang, Y., Grytsai, A., Shulga, V., Ivaniha, O. (2020). Early indications of anomalous behavior in the 2019 spring ozone hole over Antarctica. Int. J. Remote Sens. 41(19), 7530–7540. https://doi.org/10.1080/2150704X.2020.1763497.

Mitra, G., Guharay, A. (2024). Impact of sudden stratospheric warming on middle atmospheric circulation in the southern hemisphere: A comparative study. Journal of Atmospheric and Solar-Terrestrial Physics, 254, 106173. https://doi.org/10.1016/j.jastp.2024.106173.

Moustaoui M., Teitelbaum H., Valero F. P. J. (2003) Vertical displacements induced by quasi-stationary waves in the Southern Hemisphere stratosphere during spring. Mon. Wea. Rev., 131, 2279–2289. https://doi.org/10.1175/1520-0493(2003)131<2279:VDIBQW>2.0.CO;2.

Newman, P.A., Kawa, S.R., Nash E.R., 2004. On the size of the Antarctic ozone hole. Geophys. Res. Lett., 31, L21104. doi:10.1029/2004GL020596.

Newman, P.A., Nash, E.R. (2005). The unusual Southern Hemisphere stratosphere winter of 2002. J. Atmos. Sci., 62, 614–628. https://doi.org/10.1175/JAS-3323.1.

Oehrlein, J., Chiodo, G., Polvani, L.M. (2020). The effect of interactive ozone chemistry on weak and strong stratospheric polar vortex events. Atmos. Chem. Phys., 20, 10531–10544. https://doi.org/10.5194/acp-20-10531-2020.

Pazmiño, A. F., Godin-Beekmann, S., Ginzburg, M., Bekki, S., Hauchecorne, A., Piacentini, R. D., Quel, E. J. (2005). Impact of Antarctic polar vortex occurrences on total ozone and UVB radiation at southern Argentinean and Antarctic stations during 1997–2003 period. J. Geophys. Res., 110, D03103. doi:10.1029/2004JD005304.

Roy, R., Kuttippurath, J., Lefèvre, F., Kumar P. (2022). The sudden stratospheric warming and chemical ozone loss in the Antarctic winter 2019: comparison with the winters of 1988 and 2002. Theor Appl Climatol 149, 119–130. https://doi.org/10.1007/s00704-022-04031-6.

Rodas, C., Pulido, M. (2017). A climatology of Rossby wave generation in the middle atmosphere of the Southern hemisphere from MERRA reanalysis, J. Geophys. Res. Atmos., 122, 8982–8997, doi:10.1002/2017JD026597.

Sato, K., Tomikawa, Y., Hashida, G., Yamanouchi, T., Nakajima, H., Sugita, T. (2009). Longitudinally dependent ozone increase in the Antarctic polar vortex revealed by balloon and satellite observations. J. Atmos. Sci., 66, 1807–1820, doi:10.1175/2008JAS2904.1.

Safieddine, S., Bouillon, M., Paracho, A.-C., Jumelet, J., Tencé, F., Pazmino, A., Goutail, F., Wespes, C., Bekki, S., Boynard, A., Hadji-Lazaro, J., Coheur, P.-F., Hurtmans, D., Clerbaux, C. (2020). Antarctic ozone enhancement during the 2019 sudden stratospheric warming event. Geophysical Research Letters, 47, e2020GL087810. https://doi.org/10.1029/2020GL087810.

Schoeberl, M. R. (1978). Stratospheric warmings: Observations and theory. Rev. Geophys. Space Phys., 16, 521–538. https://doi.org/10.1029/RG016i004p00521.

Schoeberl, M. R., Stolarski, R. S., & Krueger, A. J. (1989). The 1988 Antarctic ozone depletion: Comparison with previous year depletions. Geophysical Research Letters, 16(5), 377–380. https://doi.org/10.1029/GL016i005p00377.

Shen, X., Wang, L., Osprey, S. (2020). The Southern Hemisphere sudden stratospheric warming of September 2019. Science Bulletin. 65, 1800–1802. https://doi.org/10.1016/j.scib.2020.06.028.

Shen, X., Wang, L., Osprey, S., Hardiman, S.C., Scaife, A.A., Ma, J. (2022). The life cycle and variability of Antarctic weak polar vortex events. J. Clim., 35, 2075–2092. https://doi.org/10.1175/JCLI-D-21-0500.1.

Shi, Y., Evtushevsky, O., Milinevsky, G., Wang, X., Klekociuk, A., Han, W., Grytsai, A., Wang, Y., Wang, L., Novosyadlyj, B., Andrienko, Y. (2024a). Impact of the 2018 major sudden stratospheric warming on weather over the midlatitude regions of Eastern Europe and East Asia. Atmospheric Research, 107112. https://doi.org/10.1016/j.atmosres.2023.107112.

Shi, G., Krochin, W., Sauvageat, E., Stober, G. (2024b). Ozone anomalies over polar regions during the stratospheric warming events. EGUsphere (preprint under discussion started on 8 March 2024). https://doi.org/10.5194/egusphere-2024-65.

Sjoberg, J.P., Birner, T. (2014). Stratospheric wave–mean flow feedbacks and sudden stratospheric warmings in a simple model forced by upward wave activity flux. J. Atmos. Sci., 71, 4055–4071. https://doi.org/10.1175/JAS-D-14-0113.1.

Stolarski, R.S. (1988). The Antarctic ozone hole. Scientific American 258(1), 30–37. https://doi.org/10.1038/scientificamerican0188-30.

Tang, L., Gu, S.-Y., Dou, X.-K. (2021) Eastward-propagating planetary waves in the polar middle atmosphere. Atmos. Chem. Phys., 21, 17495–17512. https://doi.org/10.5194/acp-21-17495-2021.

Van der A, R.J., Allaart, M.A.F., Eskes, H.J. (2015). Extended and refined multi sensor reanalysis of total ozone for the period 1970−2012. Atmos. Meas. Tech., 8, 3021–3035. https://doi.org/10.5194/amt-8-3021-2015.

Varotsos, C. (2002). The southern hemisphere ozone hole split in 2002. Environ. Sci. and Pollut. Res. 9, 375–376. https://doi.org/10.1007/BF02987584.

Veenus, V., Das, S.S. (2024). Role of Southern Hemisphere sudden stratospheric warming in altering the intensity of Brewer–Dobson circulation and its impact on stratospheric ozone and water vapor. Advances in Space Research, 73(5), 2598–2608. https://doi.org/10.1016/j.asr.2023.12.012.

Vincent, R.A., Kovalam, S., Reid, I.M., Murphy, D.J., Klekociuk, A. (2022). Southern Hemisphere stratospheric warmings and coupling to the mesosphere-lower thermosphere. J. Geophys. Res., Atmos., 127, e2022JD036558. https://doi.org/10.1029/2022JD036558.

Wang, J.C., Palo, S.E., Forbes, J.M., Marino, J., Moffat-Griffin, T., Mitchell, N.J. (2021). Unusual quasi 10-day planetary wave activity and the ionospheric response during the 2019 Southern

Hemisphere sudden stratospheric warming. J. Geophys. Res., Space Phys., 126, e2021JA029286. https://doi.org/10.1029/2021JA029286.

Wang, L., Hardiman, S.C., Bett, P.E., Comer, R.E., Kent, C., Scaife, A.A. (2020). What chance of a sudden stratospheric warming in the southern hemisphere? Environ. Res. Lett., 15, 104038. https://doi.org/10.1088/1748-9326/aba8c1.

Waugh, D.W., Randel, W.J. (1999) Climatology of Arctic and Antarctic polar vortices using elliptical diagnostics. J. Atmos. Sci., 56, 1594–1613. https://doi.org/10.1175/1520-0469(1999)056<1594:COAAAP>2.0.CO;2.

Weber, M., Dikty, S., Burrows, J.P., Garny, H., Dameris, M., Kubin, A., Abalichin, J., Langematz, U. (2011). The Brewer–Dobson circulation and total ozone from seasonal to decadal time scales. Atmos. Chem. Phys., 11, 11,221–11,235. doi:10.5194/acp-11-11221-2011.

Wei, J.C., Pan, L.L., Maddy, E., Pittman, J.V., Divarkarla, M., Xiong, X., Barnet, C. (2010). Ozone profile retrieval from an Advanced Infrared Sounder: experiments with tropopause-based climatology and optimal estimation approach. J. Atmos. Oceanic Technol., 27, 1123–1139. https://doi.org/10.1175/2010JTECHA1384.1.

Wirth, V. (1993). Quasi-stationary planetary waves in total ozone and their correlation with lower stratospheric temperature, J. Geophys. Res., 98, 8873–8882. doi:10.1029/92JD02820.

Xie, Z., Duan, A., Tian, Q. (2017). Weighted composite analysis and its application: An example using ENSO and geopotential height. Atmospheric Science Letters, 18(11), 435-440. https://doi.org/10.1002/asl.786.

Yamazaki, Y., Matthias, V. (2019). Large-amplitude quasi-10-day waves in the middle atmosphere during final warmings. J. Geophys. Res.: Atmos., 124, 9874–9892. https://doi.org/10.1029/2019JD030634.